Electronic Supplementary Information (ESI)

$FeMnO_3$: a High-Performance Li-Ion Battery Anode Material

Kangzhe Cao,[a] Huiqiao Liu, [a] Xiaohong Xu, [a] Yijing Wang,[a] and Lifang Jiao,[a, b]*

Corresponding Author

** E-mail: jiaolf@nankai.edu.cn (L.J.)*

Experimental Section

All the chemicals were purchased and used without further purification.

Material Synthesis：

$FeMnO_3$ particles were prepared by a hydrothermal method and post annealing. Typically, $MnCl_2 \cdot 6H_2O$ (2.5 mmol), $FeCl_3 \cdot 6H_2O$ (2.5 mmol), and NaOH (45 mmol) were dissolved in 50 mL distilled water by stirring for 10 min. The solution was then transferred into a 100 mL teflon-lined autoclave and maintained at 180 ^oC for 12 h. The black product was separated by centrifugation and dried for further treatment. After being annealed at 700 ^oC for 2 h in air, the $FeMnO_3$ particles were obtained. By the same procedure, Fe_2O_3 and Mn_2O_3 were synthesized using $FeCl_3 \cdot 6H_2O$ (2.5 mmol) and $MnCl_2 \cdot 6H_2O$ (2.5 mmol) as the starting material under the same conditions, respectively.

Material Characterization：

The crystal structures of the products were characterized by X-ray diffraction (XRD, Rigaku MiniFlexII, with Cu Kα radiation, λ = 1.5408 Å), and the morphology and microstructure were characterized by scanning electron microscopy (SEM; JEOL JSM-7500F) equipped with an energy dispersive spectroscopy (EDS) spectrometer and transmission electron microscopy (TEM; Philips Tecnai G2 F20). The binding energies of Fe and Mn in fresh $FeMnO_3$ were investigated by X-ray photoelectron spectroscopy (XPS; Kratos Axis Ultra DLD spectrometer), and those in the cycled $FeMnO_3$ electrode were surveyed after argon ion beam sputtering. Surface area was measured by the N_2 adsorption-desorption isotherms on ASAP 2020/Tristar 3000.

Electrochemical Measurements:

Electrochemical measurements of the $FeMnO_3$, Fe_2O_3, Mn_2O_3 particles and the mixture of Fe_2O_3 and Mn_2O_3 were carried out using a two-electrode cell assembled in an argon-filled glove box. The

working electrodes consisted of 75 wt% active material ($FeMnO_3$, Fe_2O_3, Mn_2O_3, or the mixture of Fe_2O_3 and Mn_2O_3 with different mole ratio), 15 wt% Super P carbon black, and 10 wt% sodium carboxymethyl cellulose (CMC). For the mixture electrodes, Fe_2O_3 and Mn_2O_3 with different mole ratios (including 1:2, 1:1, and 2:1) were firstly mixed totally by hand grinding in an agate mortar for 0.5 h. The loading amount of the electrode materials were balanced and measured ~0.80-0.90 mg cm^{-2} by a microbalance (Mettler, XS105DU) with an accuracy of 0.01 mg. The electrolyte was 1 M $LiPF_6$ in a mixture of ethylene carbonate (EC) and diethyl carbonate (DMC) (EC: DMC = 1:1 by volume). Pure lithium foil was used for both the counter and reference electrode. The separator was Celgard 2320 membrane. Cyclic voltammetry (CV) testing with a cut-off voltage window of 3.00-0.01 V (*vs.* Li^+-Li, 0.1 mV s^{-1}) and electrochemical impedance spectroscopy (EIS, 0.1-100k Hz) measurements were both performed on a CHI660b electrochemical workstation (Chenhua, Shanghai, China). Galvanostatic charge-discharge tests and the galvanostatic intermittent titration technique (GITT) experiment were carried out on a Land Battery Measurement system (Land CT2001A, Wuhan, China) under set current densities in the fixed voltage range of 3.00-0.01 V at room temperature. [1]

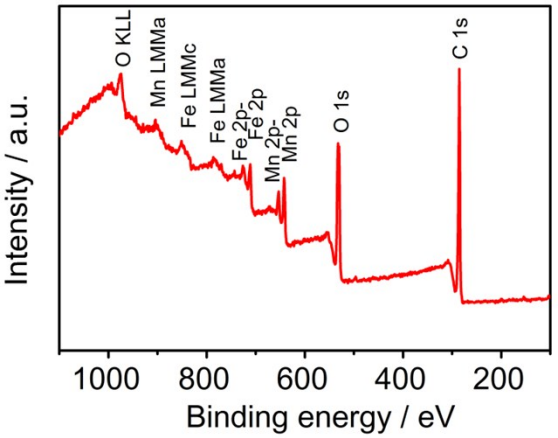

Fig. S1 Wide XPS survey spectrum of the as-prepared $FeMnO_3$ particles.

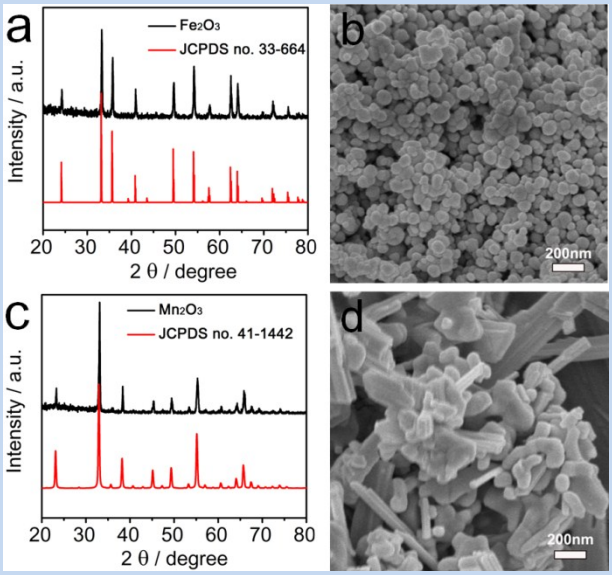

Fig. S2 XRD patterns (a, c) and SEM images (b, d) of the as-prepared Fe_2O_3 (a, b) and Mn_2O_3 (c, d) particles.

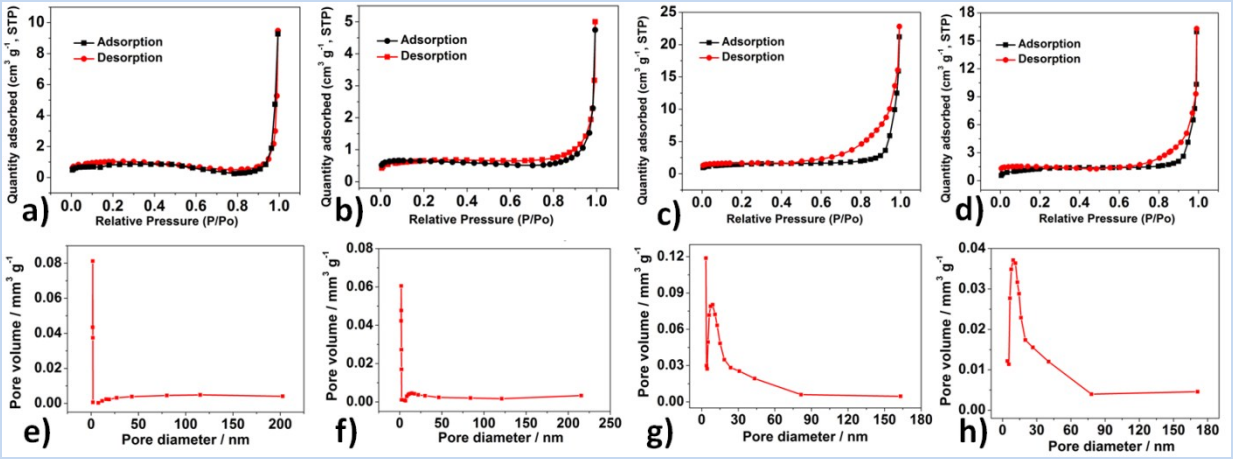

Fig. S3 N_2 adsorption-desorption isotherms (a-d) and the corresponding pore-size distribution (e-h) of the as-prepared $FeMnO_3$ (a and e), Fe_2O_3 (b and f), Mn_2O_3 (c and g) particles and the mixture of Fe_2O_3 and Mn_2O_3 with a mole ratio of 1:1 (d and h).

N_2 adsorption-desorption isotherms and the pore-size distribution of the as-prepared materials are shown in Fig. S3. Obviously, adsorption isotherm and desorption isotherm of the $FeMnO_3$ almost overlaps each other, especially on the relative pressure between 0.3 and 1.0, exhibits a type-Ⅱ isotherm with the BET surface area of 1.74 m^2 g^{-1}. This result indicates that no pores in this sample. The corresponding pore-size distribution is shown in Fig. S3e, which further confirms that no pores exist in the as-prepared $FeMnO_3$ particles. The Fe_2O_3, Mn_2O_3 and their mixture show a type-IV isotherm with an H3-type hysteresis loop.[2] Broad peaks of the pore-size distribution at 10-40 nm were found in Fig. 3f-h, corresponding to the mesopores among the particles. It should be pointed out that the pore volumes are too small, also indicating the low BET surface areas. The BET surface areas and pore sizes of the as-prepared samples are summarized in Tab. S1.

Tab. S1 The particle sizes, crystallite sizes, and BET surface area of the as-prepared $FeMnO_3$, Fe_2O_3, Mn_2O_3 nanoparticles and the mixture of Fe_2O_3 and Mn_2O_3 with a mole ratio of 1:1.

Samples	Particle sizes (nm)	Crystallite sizes (nm)	BET surface area ($m^2\ g^{-1}$)	Pore size (nm)
$FeMnO_3$	300~500	44.2	1.740	-
Fe_2O_3	80~150	53.3	3.275	15
Mn_2O_3	50~500	39.2	5.106	12
Mixture	-	-	4.456	15

The particle sizes observed from SEM images, crystallite sizes calculated by Scherrer equation, and specific surface area evaluated by N_2 adsorption-desorption isotherms were listed on Table S1. Typically, the crystallite sizes are calculated by Scherrer equation (S1) based on the strongest diffraction peak:

$$D = \frac{k\lambda}{\beta \cos\theta} \qquad \textbf{(S1)}$$

where D is the mean size of the crystallites, K is the dimensionless shape factor (0.89 in value), λ is the X-ray wavelength (1.544 Å), β is the line broadening at half maximum intensity (FWHM) in radians, and θ is the Bragg angle.

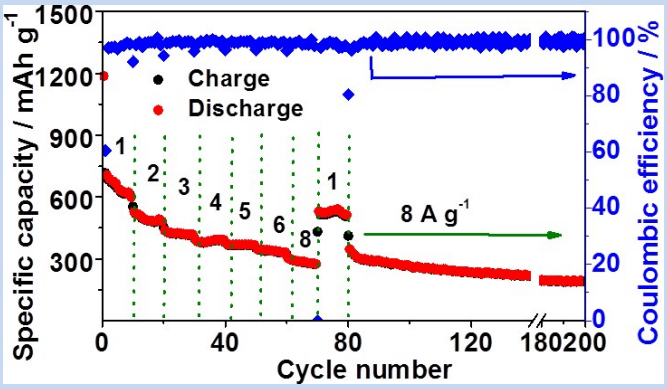

Fig. S4 Rate capability of a mixed electrode (Fe_2O_3 and Mn_2O_3 simply mixed in a molar ratio of 1:1).

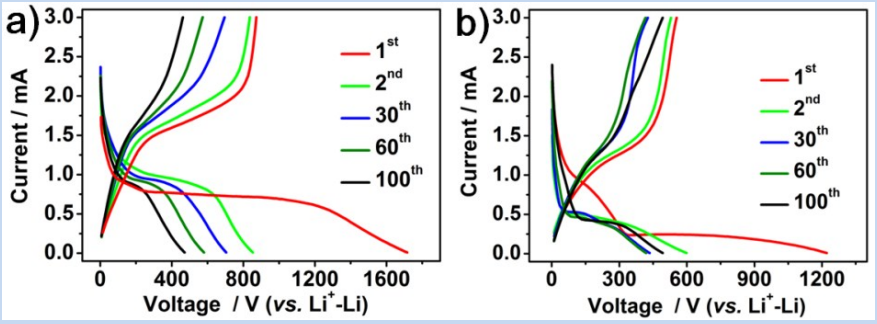

Fig. S5 Discharge-charge curves for the selected cycles of Fe_2O_3 (a) and Mn_2O_3 (b) electrodes at 1.0 A g^{-1}.

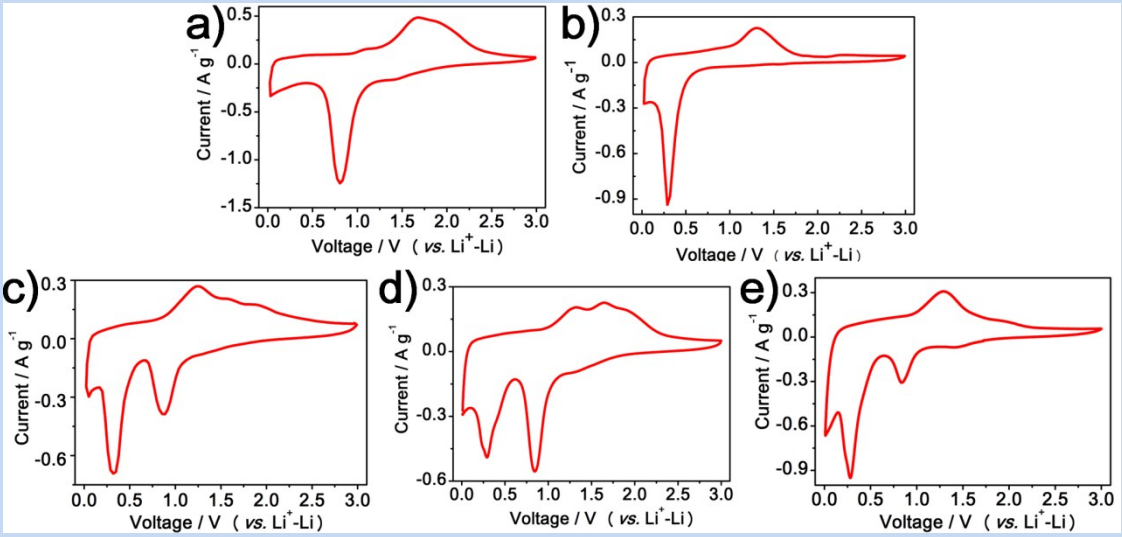

Fig. S6 CV curves for the 2nd cycle of Fe_2O_3 electrode (a), Mn_2O_3 electrode (b), and mixed electrodes (c-e, simple mixtures of Fe_2O_3 and Mn_2O_3 in different molar ratios). Fe_2O_3 to Mn_2O_3 for mixed electrodes: (c) 2:1, (d) 1:1, and (e) 1:2.

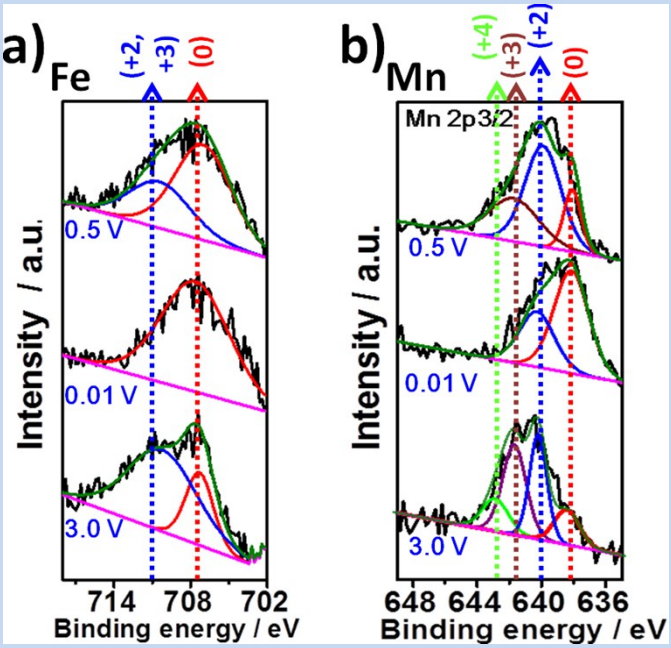

Fig. S7 XPS spectra of the cycled $FeMnO_3$ electrode at different lithiation and delithiation states: Fe $2p_{3/2}$ (a) and Mn $2p_{3/2}$ (b) at 0.5 V and 0.01 V in discharge, and 3.0 V in charge.

Tab. S2 The experimental and theoretical *d*-spacings (Å) and the corresponding Miller indices of the products at 0.5 V in discharge.

d-spacing experimental value (Å)	Fe (ref. JCPDS 1-1252)		Mn_2O_3 (ref. JCPDS 1-1061)		Mn_3O_4 (ref. JCPDS 1-1127)	
	(h l k)	*d*	(h l k)	*d*	(h l k)	*d*
2.69	-	-	2 2 2	2.68	-	-
2.35	-	-	4 0 0	2.32	0 0 4	2.36
2.1/2.06	1 1 0	2.05	-	-	2 2 0	2.03

Tab. S3 The experimental and theoretical *d*-spacings (Å) and the corresponding Miller indices of the products at 0.01 V in discharge.

d-spacing experimental value (Å)	Fe (ref. JCPDS 1-1252)		Mn (ref. JCPDS 1-1234)	
	(h l k)	*d*	(h l k)	*d*
2.06/2.08/2.09	1 1 0	2.05	2 2 1	2.10

Tab. S4 The experimental and theoretical *d*-spacings (Å) and the corresponding Miller indices of the products at 3.0 V in charge.

d-spacing experimental value (Å)	Fe_2O_3 (ref. JCPDS 1-1053)		Fe_3O_4 (ref. JCPDS 1-1111)		Mn_2O_3 (ref. JCPDS 1-1061)		Mn_3O_4 (ref. JCPDS 1-1127)	
	(h l k)	*d*	(h l k)	*d*	(h l k)	*d*	(h l k)	*d*
4.83	-	-	1 1 1	4.85	-	-	1 0 1	4.92
2.97	-	-	2 2 0	2.97	-	-	-	-
2.66	1 0 4	2.69	-	-	2 2 2	2.68	-	-
2.48	-	-	-	-	-	-	2 1 1	2.48
2.43	-	-	2 2 2	2.42				

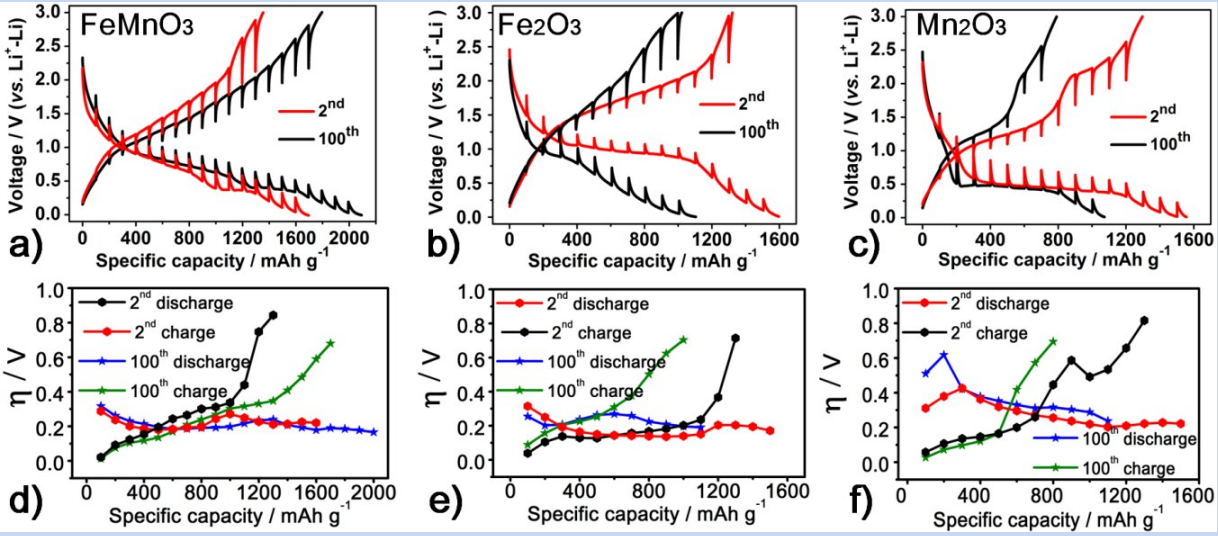

Fig. S8 GITT curves (a-c) plotted with the voltage as a function of specific capacity and (d-f) overpotential value (η) as a function of specific capacity for the selected 2nd and 100th cycle at 0.05 A g^{-1}: (a and d) $FeMnO_3$, (b and e) Fe_2O_3, and (c and f) Mn_2O_3 electrodes.

Fig. S8a-c show the discharge-charge curves at 0.05 A g^{-1} under GITT conditions in the 2nd and 100th cycles. It can be seen that the voltage hysteresis of the $FeMnO_3$ electrode is decreased and the capacity is increased, while the other two electrodes show enlarged voltage hysteresis and degraded capacity. The corresponding overpotential (η) values are shown in Figure S8d-e, and those are roughly estimated by the difference between the open circuit voltage measured after relaxation and the cut-off voltage.[3] Evidently, the η values for the $FeMnO_3$ electrode in discharge process changed little while that in charge process reduced after 100 cycles. The η values for the Fe_2O_3 and Mn_2O_3 electrodes, however, are more or less enlarged after 100 cycles. These comparison results confirm that the kinetics of Fe_2O_3 and Mn_2O_3 electrodes are diminished after long cycling while that of the $FeMnO_3$ electrode is kept in highly active.

In addition, the discharge and charge capacities in the 2nd cycle for these electrodes under the GITT condition (0.05 A g^{-1}) almost keep pace with each other, achieving a capacity of 1696 mAh g-

[1] for $FeMnO_3$ electrode, while these capacities are very different from those for each single metal oxide under the continuous galvanostatic condition (1 A g^{-1}). Moreover, the capacities achieved under GITT condition are larger than their theoretical capacities based on the conversion mechanism. The former phenomenon indicates that the $FeMnO_3$, Fe_2O_3, and Mn_2O_3 electrodes could fully react with Li during the electrochemical reactions under appropriate conditions, achieving their theoretical capabilities. The reason for the latter phenomenon is ascribed to the pseudocapacitance interfacial storage and partial reversible formation and decomposition of the SEI layer.[4] Considering the large influence of morphology and structure, the $FeMnO_3$ anode with rationally designed structure may exhibit extraordinary electrochemical characteristics.

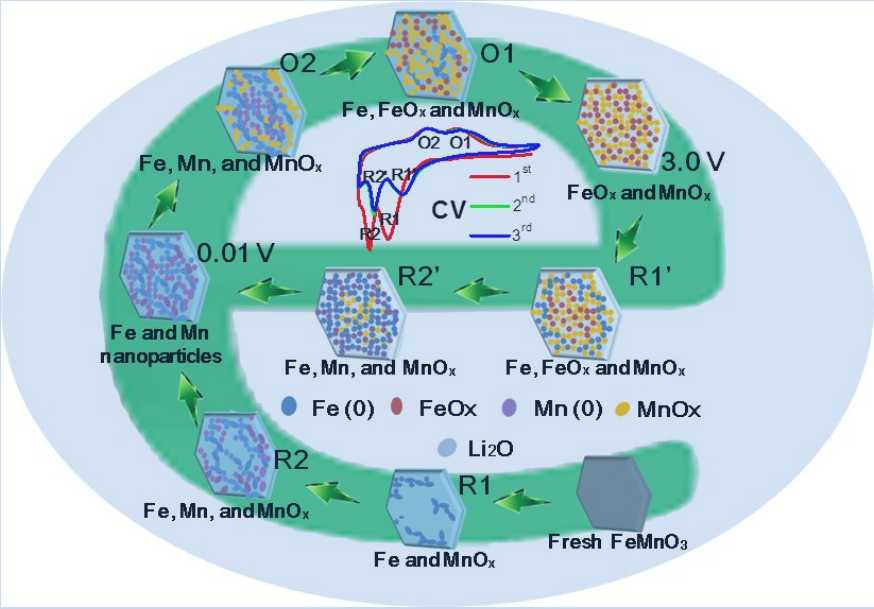

Fig. S9 Schematic illustration of the Li-storage mechanism in $FeMnO_3$ electrode.

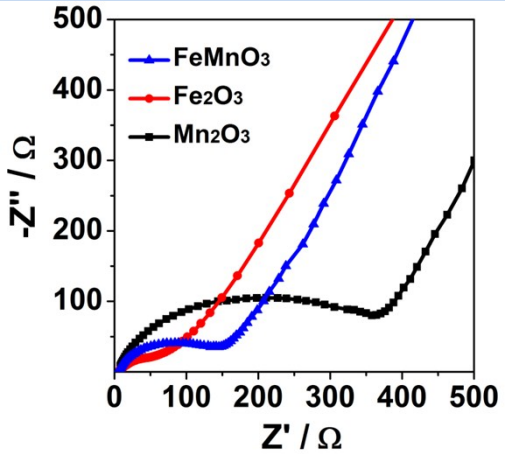

Fig. S10 Nyquist plots of the $FeMnO_3$, Fe_2O_3 and Mn_2O_3 electrodes at 1.5 V in delithiation state.

When $FeMnO_3$, Fe_2O_3, and Mn_2O_3 electrodes charged to 1.5 V, the formed Mn nanoparticles had been oxidized where the Fe nanoparticles still existed, as indicated by the CV curves of them. The charge transfer resistances (R_{ct}) in high-medium-frequency region of the $FeMnO_3$ electrode is lower than that of Mn_2O_3 electrode but larger than of Fe_2O_3 electrode, as shown in Figure S9. This result suggests that the formed Fe nanoparticles kept the high conductivity of the $FeMnO_3$ electrode when Mn nanoparticles are oxidized to MnO*x*.

References:

[1]. Z. H. Cui, X. X. Guo, H. Li, *Energy Environ. Sci.,* **2015,** *8,* 182.

[2]. S. H. Lee, S.-H. Yu, J. E. Lee, A. Jin, D. J. Lee, N. Lee, H. Jo, K. Shin, T.-Y. Ahn, Y.-W. Kim, H. Choe, Y.-E. Sung, T. Hyeon, *Nano Lett.,* **2013,** *13,* 4249; J. Kan, Y. Wang, *Sci. Rep.,* **2013,** *3,* 3502.

[3]. K. Zhong, X. Xia, B. Zhang, H. Li, Z. Wang, L. Chen, *J. Power Sources,* **2010,** *195,* 3300.

[4]. V. Augustyn, J. Come, M. A. Lowe, J. W. Kim, P.-L. Taberna, S. H. Tolbert, H. D. Abruña, P. Simon, B. Dunn, *Nat. Mater.,* **2013,** *12,* 518; K. Cao, L. Jiao, Y. Liu, H. Liu, Y. Wang, H. Yuan, *Adv. Funct. Mater.,* **2015,** *25,* 1082; K. Cao, L. Jiao, H. Xu, H. Liu, H. Kang, Y. Zhao, Y. Liu, Y. Wang, H. Yuan, *Adv. Sci.,* **2016,** *3,* 1500185.